Available online at www.sciencedirect.com

SciVerse ScienceDirect

Ceramics International 39 (2013) 5777–5783

CERAMICS INTERNATIONAL

www.elsevier.com/locate/ceramint

Structure of a macroporous silica film as an interlayer of a laminated glass

Zhijun Feng*, Jinshan Lu, Xibao Li

School of Material Science and Engineering, Nanchang Hangkong University, Nanchang 330063, China

Received 25 November 2012; received in revised form 21 December 2012; accepted 29 December 2012
Available online 9 January 2013

Abstract

A macroporous silica film (MSF) was introduced as a buffer layer of material between a silicate glass (SG) layer and a polyurethane (PU) layer to form a new aeronautic laminated glass. Structure simulations of MSF were performed using the ANSYS software. Pore models, porosity factor models, and thickness models were established. *X*-direction stress, *Y*-direction stress, and equivalent stress of the models were determined. Simulation results indicate that the pore can effectively depress shear stress on the MSF–PU interface. Moreover, maximum *X*-direction stress, maximum compressive stress, and maximum equivalent stress on the MSF–PU interface all decrease rapidly and then increase slowly by increasing film thickness.

Keywords: Laminated glass; Macroporous silica film; Structure; Simulation

1. Introduction

At present, laminated glass has established its use as a structural material in airplanes (e.g., windshield). In China, a new aeronautic laminated glass has been developed. This new glass consists of an inorganic glass layer, an elastomeric interlayer, and an organic glass layer, permanently bonded together in an autoclave under high pressure and temperature. Inorganic glass [usually silicate glass (SG)] is used as the outer layer because of its high strength and hardness, as well as its abrasion, corrosion, and heat resistance. However, inorganic glass is brittle. The interlayer is an organic film [usually polyurethane (PU)] used as an adhesive, thermal compensator, and impact buffer layer. Organic glass [usually polymethyl methacrylate (PMMA)] is used as the inner layer because of its fine toughness and low density.

As a structural material, aeronautic laminated glass is essential in addressing strength, stability, durability, and safety requirements. Peeling failure of the interface is one of the most common reasons why laminated glass is damaged without the influence of external factors. Minor and Reznik [1] reported that failure strengths of annealed laminated glass samples are equal to failure strengths of annealed monolithic glass samples with the same nominal thickness at room temperature. Norville et al. [2] established a theoretical engineering mechanics model that accounts for factors affecting laminated-glass behavior. These factors include thickness and composition of the interlayer. These researchers found that peeling failure of laminated glass mainly occurs in the interface between the glass and the interlayer. This process is mainly determined by property differences between the materials at both sides of the interface [3].

For example, in the new aeronautic laminated glass, peeling failure occurs mainly in the SG–PU interface because of property differences between inorganic glass (brittle material) and PU (plastic material).

We aim to find a physical material which has a property between inorganic glass and PU. This material will be interposed between inorganic glass and PU to solve interface peeling failure of laminated glass.

Macroporous silica film (MSF), shown in Fig. 1, achieves our goal. As shown in red in Fig. 1, MSF is introduced into the laminated glass interface between inorganic glass and PU, where peeling failure usually occurs. MSF can be successfully

*Corresponding author. Tel.: +86 791 83863101; fax: +86 791 86453203.
E-mail address: ysufzj@126.com (Z. Feng).

0272-8842/$ - see front matter © 2012 Elsevier Ltd and Techna Group S.r.l. All rights reserved.
http://dx.doi.org/10.1016/j.ceramint.2012.12.097

synthesized with a thickness ranging from micrometers to nanometers using a number of methods [4–10]. Furthermore, MSF has been applied to laminated glass to improve the performance of the glass. Suresh et al. [11] predicted acoustic transmission loss in laminated glass with porous layers.

Using MSF has three advantages. First, the physical properties of MSF possess a certain porosity factor between the properties of inorganic glass and PU. Second, the main framework of the film material is silica, which has strong adhesive tendency toward inorganic glass. Finally, when laminated glass is synthesized, PU can be perfectly introduced into the porous silica film through the pores, thus increasing adhesive force and reducing shear strength of the MSF–PU interface.

Computer-aided design is an important tool of researchers for structural design and optimization. A number of laminated glass's numerical and analytical models [12–17] have been accomplished and applied. A numerical simulation method using a computer is implemented in this paper to design and optimize MSF structure in the new aeronautic laminated glass.

2. Materials and methods

2.1. Model establishment

Three series of numerical models with porous silica film were established [18,19] using the ANSYS software. The first series of models was the pore model consisting of SG, MSF, and PU. The following five submodels were included in the pore model: non-pore model, model of the pore on the SG–MSF interface, model of the closed pore in the silica film, model of the pore on the MSF–PU interface, and model of the pore through the silica film. The ratio of pore area to submodel area was 30%. The second series of models was the porosity factor model consisting of SG, MSF, PU, and PMMA. Seven submodels, with porosity factors from 10% to 70%, were included in the porosity factor model. The third series of models was the thickness model, which also consists of SG, MSF, PU, and PMMA. Seven submodels, with porous silica film thickness ranging from 0 μm to 50 μm, were included in the thickness model. The detailed sizes of the models are shown in Table 1.

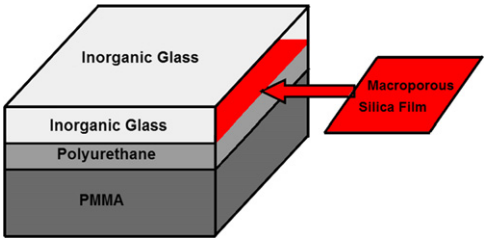

Fig. 1. Structural diagram of SG, MSF, PU, and PMMA. (For interpretation of the references to color in this figure, the reader is referred to the web version of this article.)

2.2. Physical properties

The mechanical parameters of the models are shown in Table 2. In the pore model, the elastic modulus (E) and Poisson ratio (v) of air were both zero if air is present in the pores. In the porosity factor model and the thickness model, E and v of MSF were both calculated according to the property formula of multiple materials. In the thickness model, the porosity factor of MSF is 30%.

2.3. Boundary conditions

The displacement boundary condition is as follows [15]: At the sides of the models, $\frac{\partial u}{\partial x} = 0$; $\frac{\partial v}{\partial y} = 0$.

Pressure boundary condition is as follows: At the external face of inorganic glass, 1 atm (1.013×10^5 Pa).

3. Results and discussion

3.1. Porous shape

Fig. 2 shows simulation results of X-direction (length direction) stress of the pore models. The color scale indicates X-direction stress values. Stress values less than zero at the left side of the color scale represent contraction stress toward the model center; whereas, stress values greater than zero at the right side of the color scale represent expansion stress away from the model center.

In Fig. 2(a)–(e), a minimum length of the red regions is evident in Fig. 2(e) at the SG–MSF interface, which is an interface of major concern. Thus, this observation

Table 1
Sizes of the models.

		SG	MSF	PU	PMMA
Pore model	Length	10 μm	10 μm	10 μm	
	Thickness	3 μm	10 μm	3 μm	
Porosity factor model	Length	0.1 m	0.1 m	0.1 m	0.1 m
	Thickness	5 mm	10 μm	3 mm	10 mm
Thickness model	Length	0.1 m	0.1 m	0.1 m	0.1 m
	Thickness	5 mm	0, 1, 5, 10, 20, 35, 50 μm	3 mm	10 mm

indicates that model of the pore through the silica film has minimum interfacial shear stress caused by both interface sides of expansion stress and contraction stress. However, the areas of the red regions in Fig. 2(e) at the SG are only less than those in Fig. 2(b). This observation shows that the through-pore model has higher expansion stresses at the SG then else models except model of the pore on the SG–MSF interface. On the MSF–PU interface, another interface of major concern, the lengths of the red regions in the porous model are less than those in the non-porous model, thus showing that the pore will depress shear stress on the MSF–PU interface.

Fig. 3 shows the simulation result of the series of pore models examining *Y*-direction (thickness direction) stress. The color scale indicates the value of *Y*-direction stress. Stress values less than zero at the left side of the color scale represent compressive stress; whereas stress values greater than zero at the right side of the color scale represent tensile stress.

Table 2
E and *v* of the models.

		SG	MSF	PU	PMMA
Pore model	*E* (GPa)	74.5	72.5	3.09	
	v	0.25	0.17	0.47	
Porosity factor model	*E* (GPa)	74.5	$72.5-70.995\times a$	3.09	3.85
	v	0.25	$0.17+0.315\times a$	0.47	0.32
Thickness model	*E* (GPa)	74.5	51.2	3.09	3.85
	v	0.25	0.26	0.47	0.32

a is the porosity factor.

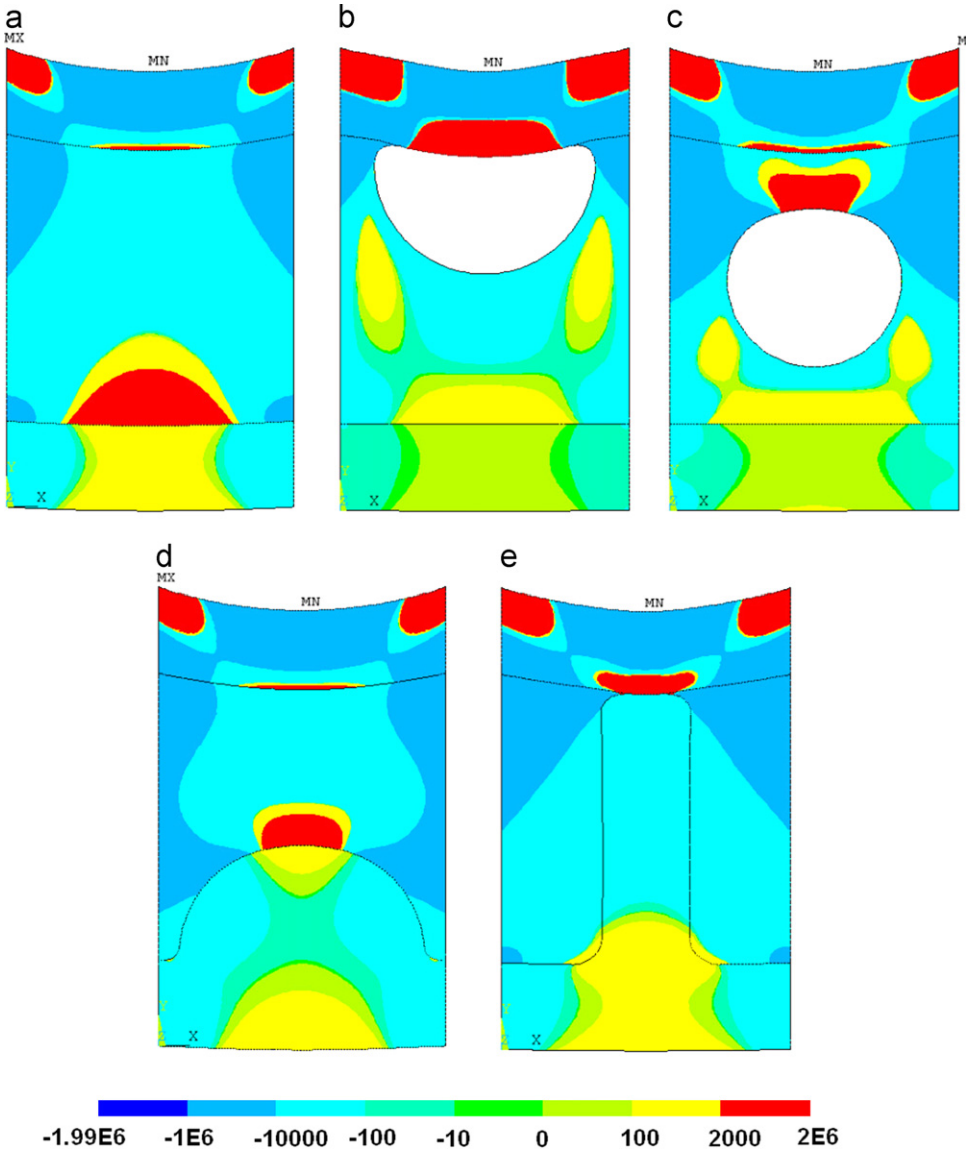

Fig. 2. *X*-direction stress of the pore models. (a) Non-pore in the model; (b) pore on the SG–MSF interface; (c) closed pore in the silica film; (d) pore on the MSF–PU interface; (e) pore through the silica film. (For interpretation of the references to color in this figure, the reader is referred to the web version of this article.)

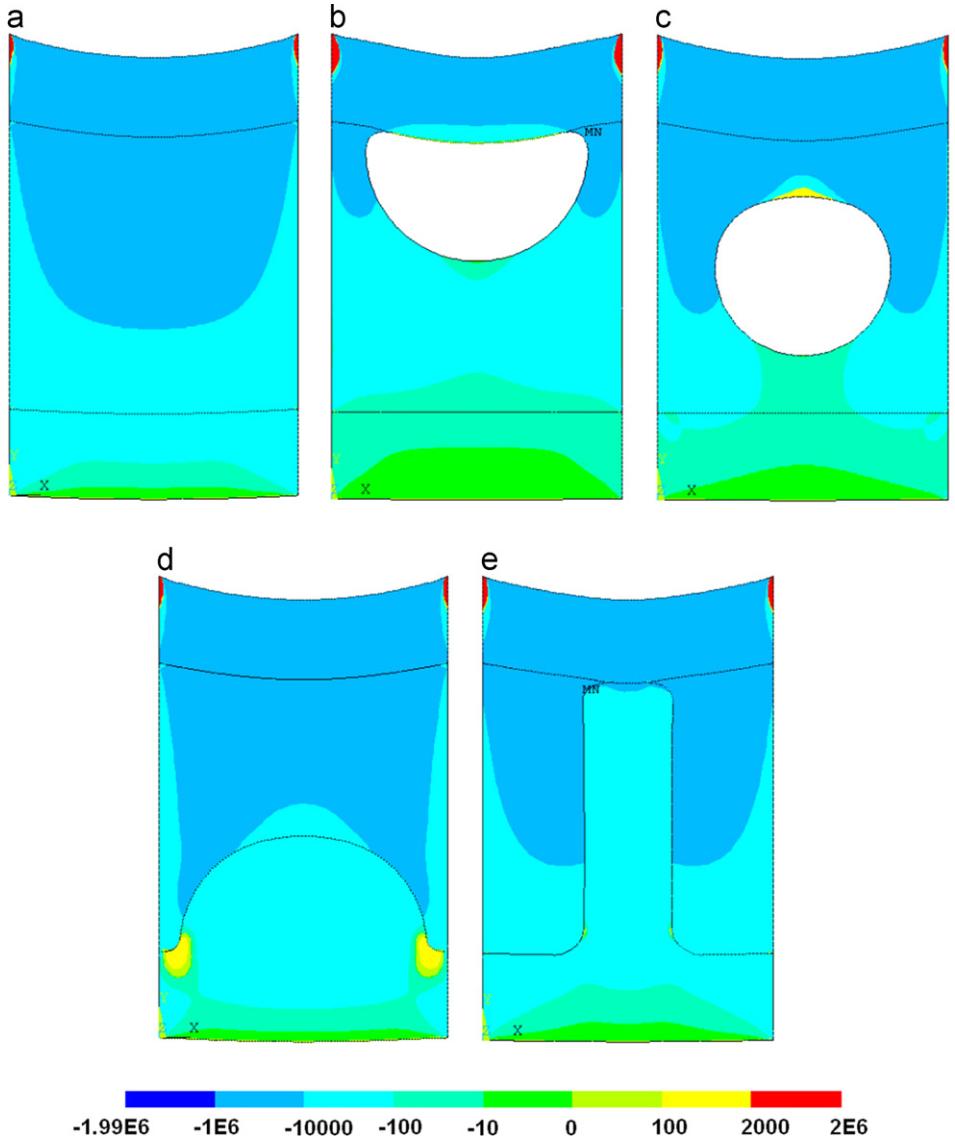

Fig. 3. *Y*-direction stress of pore models. (a) Non-pore in the model; (b) pore on the SG–MSF interface; (c) closed pore in the silica film; (d) pore on the MSF–PU interface; (e) pore through the silica film. (For interpretation of the references to color in this figure, the reader is referred to the web version of this article.)

In Fig. 3(a)–(e), a minimum length of the azure region is evident in Fig. 3(b) on the SG–MSF interface, indicating that the pore model on the SG–MSF interface has a minimum interface compressive stress. Compressive stress on the MSF–PU interface increases from left to right as follows: Fig. 3(e) < (d) < (a) < (c) < (b). Moreover, the through-pore model is observed to be the least prone to peeling failure. However, in Fig. 3(d), tensile stresses are present on the MSF–PU interface, indicating risk of failure. In addition, compared with other models, the length of the MSF–PU interface in Fig. 3(d) and (e) greatly increased. This result indicates that the bond strength of the interface in these two models has increased and that the risk of interface peeling failure has been reduced. Based on the aforementioned analyses, the pores in the porous silica film should be as far as the through-pore or the pore on the MSF–PU interface.

3.2. Porosity factor

Fig. 4 shows *X*-direction stresses for the seven simulation results for different porosity factor models along the length direction at the MSF–PU interface. Positive stresses are expansion stresses along the length direction at the interface center. Negative velocities are contraction stresses at the interface sides.

In Fig. 4, the values of *X*-direction stress decrease on the MSF–PU interface as porosity factor of porous silica film increases. Reduction of the *X*-direction stress indicates that the tendency of interface slippage caused by shearing is reduced. Furthermore, the forced condition of the interface improved in the horizontal direction. This improvement is caused by increasing porosity factor. Material properties (E and v) of the porous silica film at one interface side gradually become

closer to the performance parameters of the PU at the other interface side. Thus, the decreasing difference of material performance at both interface sides causes the decreasing interfacial shear stress by different strains on both interface sides. In other words, the increasing film porosity factor is significant in reducing risk of interface peeling invalidation by shear slip.

Fig. 5 shows *Y*-direction stresses on the MSF–PU interface of porosity factor models. Positive stresses are tensile stress. Negative velocities are compressive stress. Maximum compressive stress at both sides of the model is evident in Fig. 5(a), and tensile stress is close to maximum compressive stress. Distribution results in Fig. 5(a) are consistent with those reported in literature [1,2]. Simulation results of other porosity factor models are similar with Fig. 5(a). In Fig. 5(b), maximum compressive stress and maximum tensile stress on the MSF–PU interface are observed to increase initially and then decrease with increasing porosity factor. This behavior is caused by v of porous silica with a porosity factor lower than that of inorganic glass, which results in decreasing cross-sectional deformations of the interface and then increasing compressive stress and tensile stress of the interface. v of porous silica gradually increases with increasing porosity factor. When porosity factor is more than 25.4%, v of porous silica will be between that of inorganic glass and PU. Furthermore, the physical properties of porous silica will just be the original structural design requirements of inset materials. Thus, compressive stress and tensile stress of the interface begin to decrease gradually with increasing porosity factor. If the interface of laminated glass exerted a large compressive stress and a small tensile stress, the glass will be difficult to destroy. Therefore, porosity factor of porous silica film should not be too large. As previously described, the suitable porosity factor of porous silica film should be 30–40%.

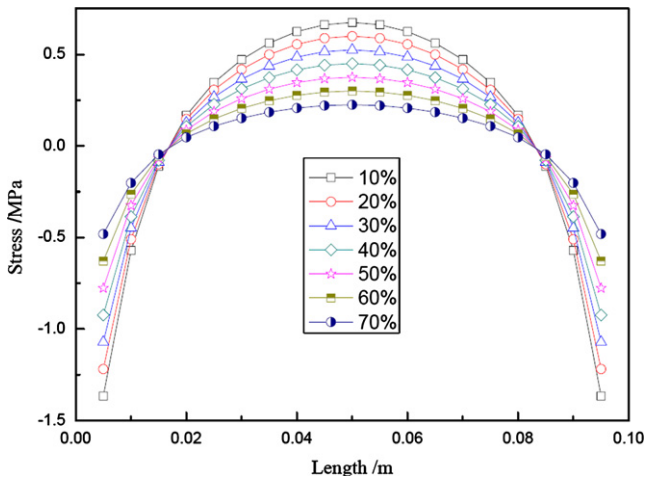

Fig. 4. Distribution of *X*-direction stress along the length of porosity factor models on the MSF–PU interface.

3.3. Film thickness

Fig. 6 shows maximum *X*-direction stress with the thickness of porous silica film in the thickness models. The inset in Fig. 6 shows the distribution of *X*-direction stress on the MSF–PU interface when film thickness is 10 μm.

In the inset in Fig. 6, the distribution of *X*-direction stress on the interface is similar to that in Fig. 4, and maximum *X*-direction stress is at both sides of the model. Simulation results of other thickness models are similar to the inset in Fig. 6. In Fig. 6, *X*-direction stress decreases rapidly and then increases slowly with increasing thickness of MSF. This behavior is caused by the change which occurs from a single interface (SG–PU) to two new interfaces (SG–MSF, MSF–PU) when MSF is inserted between inorganic glass and PU. Therefore, physical performance differences of the material on both sides of the two new interfaces are much smaller than those of the original single interface. Thus, *X*-direction stress decreases rapidly. Relative strain of the film along the thickness direction decreases, and *X*-direction stress increases slowly with increasing film thickness. Accordingly, the low thickness of the film contributes in reducing shear stress on the MSF–PU interface.

Fig. 7 shows *Y*-direction stress and equivalent stress on the MSF–PU interface of the thickness models. The distribution of *Y*-direction stress in Fig. 7 is similar to that in Fig. 5(a). Moreover, maximum compressive stress is present at both

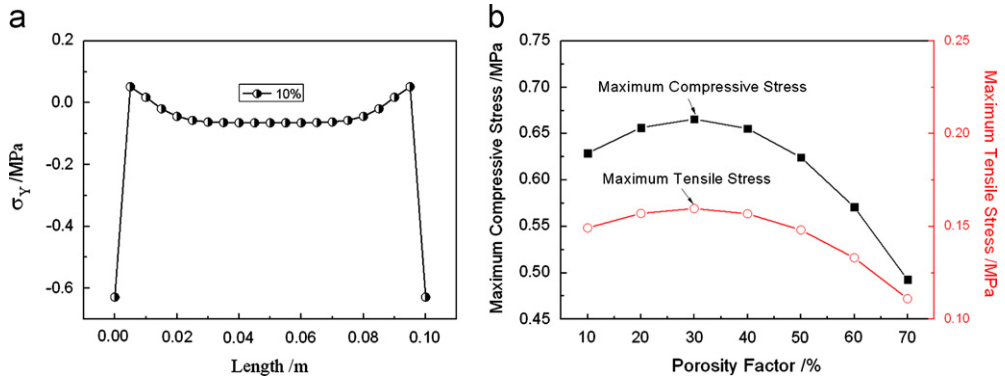

Fig. 5. *Y*-direction stress of porosity factor models on the MSF–PU interface. (a) Distribution of *Y*-direction stress along interface length when porosity factor is 10%; (b) maximum compressive stress and maximum tensile stress with the porosity factor.

sides of the model. Equivalent stress is symmetrical on the interface, and maximum equivalent stress is also present at both sides of the model. Equivalent stress, also known as von Mises stress, is computed using the von Mises yield criterion. Simulation results of the other thickness models are similar with that in Fig. 7(a). In Fig. 7(b), both maximum compressive stress and maximum equivalent stress on the MSF–PU interface decrease rapidly and then increase slowly with increasing film thickness. The reason for the area where maximum compressive stress decreased rapidly is similar to the analysis of the same area in Fig. 6. Relative strain of the film along the thickness direction decreases with increasing film thickness. v remains constant, whereas relative strain of the film along the length direction also decreases. Furthermore, deformation areas of the cross section in the film are slowly reduced, and maximum compressive stress increases slowly. Equivalent stress is equal to the resultant stress of X-direction and Y-direction stresses. The same variety of maximum X-direction stress and maximum Y-direction stress is observed with film thickness. Therefore, maximum equivalent stress decreases rapidly and then increases slowly with increasing film thickness. Reduction of maximum compressive stress is detrimental to the stability of laminated glass. Therefore, film thickness of porous silica film should not be too small. Combined with the preparation of porous silica film and the post-molding of laminated glass, the suitable thickness of porous silica film should be around 10 μm.

Fig. 8 shows a micrograph of the MSF made on the SG based on simulation results. The porosity factor of MSF is 31.2% and its thickness is 9.6 μm.

4. Conclusion

The effects of pore location, porosity factor, and film thickness on stress distribution of MSF in the aeronautic laminated glass were investigated using numerical simulations. Simulation results indicate that the pores in MSF should be as far as the through-pore or the pore on the MSF–PU interface. The pore would depress the shear stress on the MSF–PU interface. X-direction stress decreases on the MSF–PU interface, whereas maximum tensile stress on the MSF–PU interface initially increases and then decreases with increasing porosity factor. Therefore, the suitable porosity factor of MSF should be between 30% and 40%. Moreover, maximum X-direction stress, maximum compressive stress, and maximum equivalent stress on the MSF–PU interface all decrease rapidly and then increase slowly with increasing film thickness. Hence, the suitable thickness of the porous silica film should be around 10 μm.

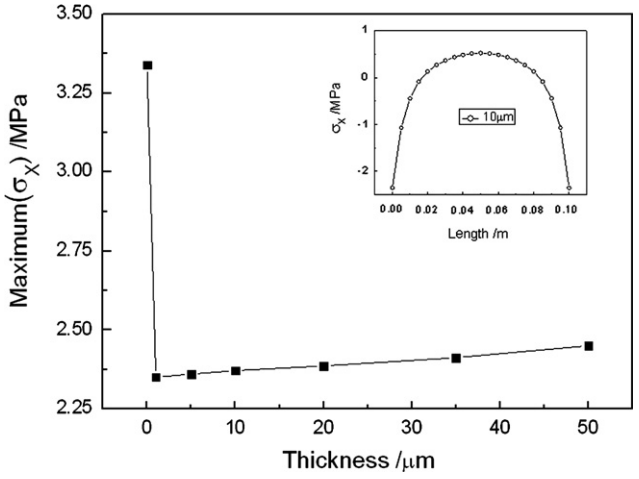

Fig. 6. Maximum X-direction stress with the porous silica film thickness.

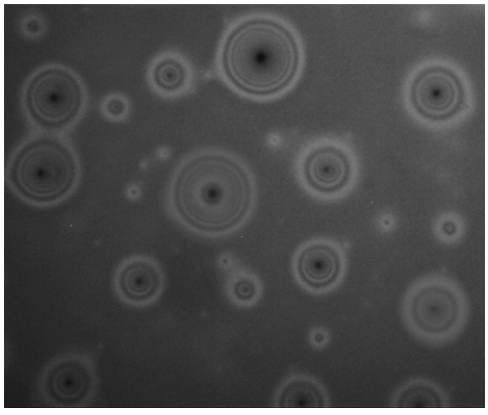

Fig. 8. MSF micrograph.

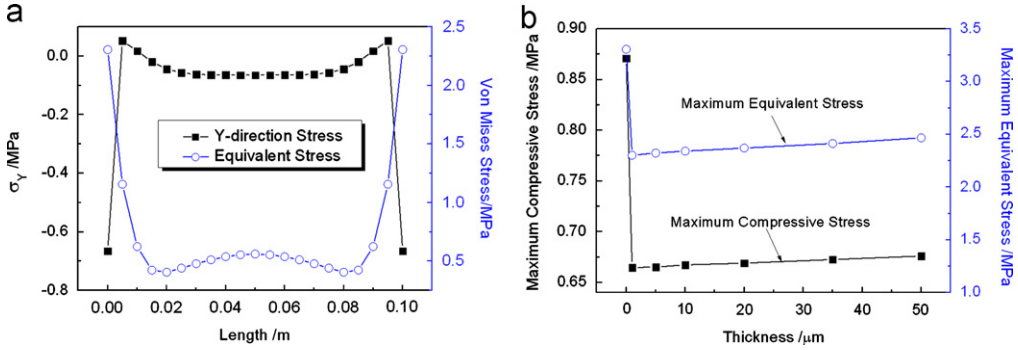

Fig. 7. Y-direction stress and equivalent stress of thickness models on the MSF–PU interface. (a) Distribution of Y-direction stress and equivalent stress along the interface length when the thickness is 10 μm; (b) maximum compressive stress and maximum equivalent stress with film thickness.

Acknowledgments

The authors wish to acknowledge the Aeronautical Science Foundation of China (BA201101357) for the financial support, and thank Wangzi Liu providing the experimental micrograph. The Startup Foundation for Doctors of Nanchang Hangkong University (EA200901373) is also gratefully acknowledged for supporting this study.

References

[1] J. Minor, P. Reznik, Failure strengths of laminated glass, Journal of Structural Engineering 116 (1990) 1030–1039.
[2] H.S. Norville, K. King, J.L. Swofford, Behavior and strength of laminated glass, Journal of Engineering Mechanics 124 (1998) 46–53.
[3] A. Duser, A. Jagota, S. Bennison, Analysis of glass/polyvinyl butyral laminates subjected to uniform pressure, Journal of Engineering Mechanics 125 (1999) 435–442.
[4] R. Cademartiri, M.A. Brook, R. Pelton, J.D. Brennan, Macroporous silica using a sticky Stöber process, Journal of Materials Chemistry 19 (2009) 1583–1592.
[5] D.L. Sun, X.C. Yu, W.J. Liu, D.B. Sun, Laminated biomorphous SiC/Si porous ceramics made from wood veneer, Materials & Design 34 (2012) 528–532.
[6] A.Y. Zhang, W.J. Xue, Z.F. Chai, Synthesis of a macroporous silica-based derivative of pyridine material and its application in separation of palladium, AIChE Journal 56 (2010) 3074–3083.
[7] Y.S. Cho, S.Y. Choi, Y.K. Kim, G.R. Yi, Bulk synthesis of ordered macroporous silica particles for superhydrophobic coatings, Journal of Colloid and Interface Science 386 (2012) 88–98.
[8] T. Förster, S. Scholz, Y.Z. Zhu, J.A. Lercher, One step synthesis of organofunctionalized transition metal containing meso- and macroporous silica spheres, Microporous and Mesoporous Materials 142 (2012) 464–472.
[9] A.Y. Zhang, W.J. Xue, Z.F. Chai, Preparation of a macroporous silica–pyridine multidentate material and its adsorption behavior for some typical elements, AIChE Journal 58 (2012) 3517–3525.
[10] D.J. Yang, Y. Xu, W.J. Xu, D. Wu, Y.H. Sun, H.Y. Zhu, Tuning pore size and hydrophobicity of macroporous hybrid silica films with high optical transmittance by a non-template route, Journal of Materials Chemistry 18 (2008) 5557–5562.
[11] S. Suresh, T.C. Lim, J. Kastner, Predicting acoustic transmission loss through laminated glass with air and porous layers, International Journal of Vehicle Noise and Vibration 8 (2012) 237–260.
[12] J. Minor, H. Norville, Design of window glass for lateral pressures, Journal of Architectural Engineering 12 (2006) 116–121.
[13] M. Timmel, S. Kolling, P. Osterrieder, P.A.D. Bois, A finite element model for impact simulation with laminated glass, International Journal of Impact Engineering 34 (2007) 1465–1478.
[14] P. Foraboschi, Behavior and failure strength of laminated glass beams, Journal of Engineering Mechanics 133 (2007) 1290–1301.
[15] D. Weggel, B. Zapata, Laminated glass curtain walls and laminated glass lites subjected to low-level blast loading, Journal of Structural Engineering 134 (2008) 466–477.
[16] S. Bati, G. Ranocchiai, C. Reale, L. Rovero, Time-dependent behavior of laminated glass, Journal of Materials in Civil Engineering 22 (2010) 389–396.
[17] P. Foraboschi, Analytical model for laminated-glass plate, Composites Part B—Engineering 43 (2012) 2094–2106.
[18] L. Galuppi, F.R. Gianni, Effective thickness of laminated glass beams: new expression via a variational approach, Engineering Structures 38 (2012) 53–67.
[19] L. Galuppi, F.R. Gianni, The effective thickness of laminated glass plates, Journal of Mechanics of Materials and Structures 7 (2012) 375–400.